Geotextiles and Geomembranes 52 (2024) 574–584

Contents lists available at ScienceDirect

Geotextiles and Geomembranes

journal homepage: www.elsevier.com/locate/geotexmem

Regular Paper

Experimental evaluation of geosynthetic-modular block connection loads

F.H.M. Portelinha [a,*], P.V.C. Figueiredo [b], J.G. Zornberg [c]

[a] Federal University of Sao Carlos, Civil Engineering Department, Washington Luis Rd., km 235, Sao Carlos, Sao Paulo 13.565-905, Brazil
[b] Federal University of Sao Carlos, Civil Engineering Postgraduation Program, Washington Luis Rd., km 235, Sao Carlos, Sao Paulo, 13.565-905, Brazil
[c] The University of Texas at Austin, Civil Engineering Department – GEO, 1 University Station C1792 Austin, TX 78712-0280, USA

ARTICLE INFO

Keywords:
Geosynthetics
Facing
Connection loads
Modular blocks
Down-drag

ABSTRACT

The design of segmental geosynthetic mechanically stabilized walls with masonry block facing is often governed by the loads that develop at the connection between the facing and geosynthetic. Yet the current understanding of the mechanisms involved in the mobilization of such connection loads is, at best, incomplete. The testing apparatus developed as part of this study facilitates simulating the transference of stresses at the face and evaluating the facing connection loads in geosynthetic-reinforced soil walls. This study assesses the connection loads between a geogrid reinforcement connected frictionally to modular concrete blocks. A comprehensive instrumentation program was implemented to capture lateral earth pressures, geosynthetic strains and loads acting at the geogrid-block connection in a geosynthetic-reinforced unit cell subjected to incremental surcharge stages. Results indicate that conventional calculations, based on earth pressure theory, may underestimate the facing connection loads, mainly when the connection loads are triggered by the differential settlement of the backfill relative to the block facing. When this mechanism dominates the mobilization at the connection, reinforcement loads increase as the differential settlement increases, developing down-drag forces at the connection between the geogrid and modular blocks.

1. Introduction

Geosynthetic Mechanically Stabilized Earth (GMSE) walls, constructed with masonry block facing, have been used in permanent applications, including critical structures such as extremely tall retaining walls (exceeding 30 m in height) and bridge abutments. A key consideration in the design of these structures is the evaluation of modes of failure including the connection loads that develop between a geosynthetic reinforcement and modular blocks. Specifically, facing failures have been documented to occur when the connection loads on the facing exceed the capacity of the connection (Bathurst, 2005; Koerner and Koerner, 2018; Xu et al., 2020; Morsy, 2021). In segmental GMSE structures, the geosynthetic reinforcement may be connected to the wall facing at the front of the wall, either through the friction that develops between the geosynthetic and modular blocks, or via structural elements to provide a mechanical connection (Simac, 1990). Facing design requires the availability of adequate connection strength, which should offer a sufficient margin of safety against failure. This margin of safety is often defined as the allowable connection strength over the required connection strength. (AASHTO, 2020; Elias et al., 2001; Berg et al., 2009; Collin, 1997). The allowable connection strength is rapidly becoming available and can be obtained from pullout tests (Simac et al., 1993; Bathurst et al., 1993; ASTM D6638, 2018; Bathurst and Huang, 2010). Historically, the first specification for testing modular concrete-geosynthetic connection strength was test method GS-8 published by the Geotechnical Research Institute (GRI, 1991). After testing developments by Bathurst and Simac (1993), connection test protocols were then promulgated in the NCMA (Simac et al., 1993) and currently in ASTM D6638. The shear capacity testing of segmental concrete units was first introduced by the GRI in test method GS9 and originally promulgated in the NCMA manual produced by Simac et al. (1993). It served as the basis for the current standard ASTM D6916 after an important experimental contribution developed by Bathurst et al. (2008a).

More challenging than obtaining the allowable connection strength is predicting the required connection strength. Task Force 27 (1990), an industry-wide group, was among the first to recommend that the required connection strength be equal to the design geosynthetic strength in the backfill, as referenced by Bathurst et al. (1993). Similarly, AASHTO (2020) recommends using 100% of the reinforcement

* Corresponding author.
E-mail addresses: fportelinha@ufscar.br (F.H.M. Portelinha), paulovcarvalho15@gmail.com (P.V.C. Figueiredo), zornberg@mail.utexas.edu (J.G. Zornberg).

https://doi.org/10.1016/j.geotexmem.2024.03.001
Received 4 August 2023; Received in revised form 27 February 2024; Accepted 2 March 2024
Available online 13 March 2024

design strength at the bottom of the wall, while linearly decreasing the required connection strength to 73% at the top of the wall. More recently, the LRFD Bridge Design Specifications (AASHTO, 2020) suggest that the nominal tensile load applied to the soil reinforcement connection at the wall face, denoted as T_o, should be equal to the nominal reinforcement tension, denoted as T_{max}, for all wall systems, regardless of facing and reinforcement type. In the limit equilibrium design framework of Leshchinsky et al. (2016), a rational solution is provided to determine the connection load, which typically results in nonlinear values along the structure height and lower magnitudes in relation to the maximum reinforcement load mobilized in the backfill. For closely-spaced reinforcement systems, Wu (2001) recommends a lateral earth pressure acting at the facing of 72% of the active lateral earth pressure, while Soong and Koerner (1997) suggest 50%.

Unfortunately, all previously mentioned recommendations are controversial and unsubstantiated based on true mechanism(s). Ideally, the required connection strength would be defined not only considering lateral earth pressures but also short-term construction issues, such as the details of wall construction, facing type and construction quality, and long-term phenomena that may occur over the service lifetime of a wall system. For example, Allen and Bathurst (2014a, 2014b) measured the connection loads in actual full-scale production walls and found them to be the maximum tensile loads, reaching values around 30% higher than the load mobilized in the backfill. This was generally observed to occur at upper reinforced layers, while at lower layers the connection loads were between 50 and 70% of the maximum tensile load in the backfill. Based on MSE instrumented field walls, Bathurst et al. (2007) demonstrated a tendency for peak strains to occur near the back of the facing due to downward soil movement during compaction in relation to the hard face. Riccio et al. (2014) also measured connection loads equal to or greater than the maximum tensile loads in the backfill of a block-faced geogrid wall constructed with fine-grained soil. However, controversially, the maximum tensile loads occurring at the face were measured at the bottom rather than the top layers. Some authors state that the distribution of lateral earth pressures developing behind the wall facing can be viewed as acting independently in individual reinforcement layers (Wu, 20,021, Soong and Koerner, 1997; Adams and Nicks, 2018), so the magnitude primarily depends on the reinforcement spacing. However, based on an evaluation of monitored field structures, Gebremariam et al. (2020) demonstrated that the stresses acting at the face were higher than the lateral earth pressures calculated in individual layers. Nonetheless, they found a uniform stress distribution along the height of the structure in a field wall, which is expected in this type of design approach. In addition to the experimental observations reported herein, numerous cases of facing failures reported in the literature by Koerner and Koerner (2018) provide evidence that the required connection loads are typically underestimated.

Soong and Koerner (1997) indicate the placement of soil surcharge or live loadings on the surface of the backfill soil behind the wall facing, backfill and foundation settlements, and loss of soil as significant sources of stresses behind facing blocks. In the short-term, settlement of the fill behind the block facing may also be caused by the outward rotation to attain active stress conditions, poor compaction, and hydro compaction due to water infiltration causing soil to consolidate. These processes can collectively generate deformation patterns leading to additional sources of connection loads, which are related to the differential settlements between facing and backfill. In this context, Bathurst et al. (2007) and Salem et al. (2018) discussed that the cause of maximum tensile loads on reinforcements occurring at the facing, rather than within the backfill, is attributed to the out-of-plane straining of the geosynthetic reinforcement. This phenomenon, referred to by some researchers as the "down-drag effect," was reported to be a consequence of construction-related issues.

Given the challenges associated with accurately measuring connection loads in the field to further develop this topic, laboratory observations that could provide additional insight into this issue would be particularly beneficial. The present paper describes the development of a device specifically designed to assess the facing connection load within GMSE walls. Its primary goal is to gather experimental data to expand comprehension and quantify the influence of lateral earth pressures and down-drag forces on connection loads prompted by the placement of a surcharge behind the block facing. This study focuses on employing a testing arrangement developed to simulate the mechanisms inherent in a segmental GMSE structure to measure the effect of these mechanisms on connection loads, with particular emphasis on outward rotation to replicate active stress conditions.

2. Experimental program

2.1. Testing equipment and instrumentation

The testing device developed for this study consisted of a reinforced soil unit cell to simulate the stress-strain behavior occurring in the different components behind the facing of masonry block GMSE walls. Because potential failure surfaces associated with the internal stability of Geosynthetic-Reinforced Soil (GRS) walls are not typically located near wall facings, the equipment was developed to simulate the lateral earth pressures occurring under actual working stress conditions. Fig. 1a illustrates the internal mechanisms at the reinforcement-modular block interface simulated by the testing device, while Fig. 1b depicts what the testing device represents inside a GMSE wall. The lateral earth pressures acting on the facing depend on the applied surcharge levels and geosynthetic stiffness and, consequently, on the level of strains occurring in this region. In addition, the down-drag mechanism caused by differential settlements between the facing and backfill is also indicated in Fig. 1b. The down-drag effect mainly involves the reinforcement bending due to the differential settlements between the backfill soil and block facing wall. When the soil at the back of the face has higher settlements than the facing wall, down-drag forces are assumed to develop, and the mechanisms involved in the connection change. The magnitude of these changes depends on many factors including block configuration; infill soil for the block, behind the block and behind the gravel face drain; and reinforcement type, strength and stiffness. In this investigation, the connection behavior is evaluated for a rectangular block unit with a sand backfill soil and woven geogrid to provide insight into the responses of the proposed testing device.

The equipment (illustrated in Fig. 2) consists of a rigid metal box, with internal dimensions of 800 mm × 750 mm × 700 mm (width × length × height), at the front of which a geosynthetic reinforcement is placed between two compacted soil layers connected to modular blocks. For this study, the connection between the blocks and geosynthetic reinforcement is entirely frictional. The use of structural pins, often applied in practice, is understood to lead to better connection resistance. However, adopting structural pins would not allow for the characterization of the geogrid strain along the length embedded between blocks using extensometers. One lateral wall of the box consists of transparent glass, which was implemented for observation of the field displacements within the soil mass and geosynthetic layer. The constraint provided by the lateral walls implies that the boundary conditions of the soil–geosynthetic-block system are well defined by zero displacement. The back and lateral walls of the test box are lubricated with a double layer of grease and plastic sheet to minimize friction. The modular block wall was constructed over a cart that can move freely in the horizontal direction via ball bearings on rails at the bottom of the metal box. The reinforced soil mass is loaded vertically using airbags extending over the entire surface of the soil mass as well as over the modular concrete blocks. The front half of the airbag is also lubricated with grease to minimize friction between the airbag-soil-block interfaces. The movement of the front cart induces an internal strain that depends on the strain compatibility of the soil and geosynthetic reinforcement. The geosynthetic reinforcement is clamped at the back wall of the test box, an approach adopted to restrict the reinforcement displacement and

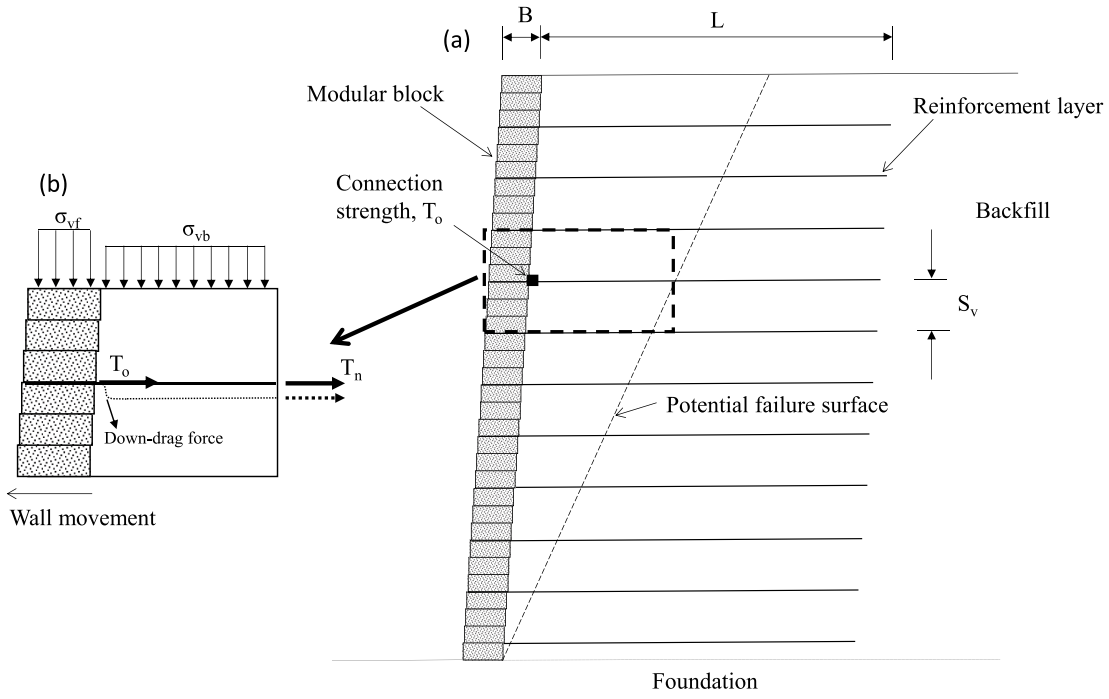

Fig. 1. Working stress conditions at facing of segmental geosynthetic MSE walls: (a) indication of condition simulated by testing device in a MSE wall; (b) internal mechanisms at the reinforcement-modular block interface simulated by the testing device.

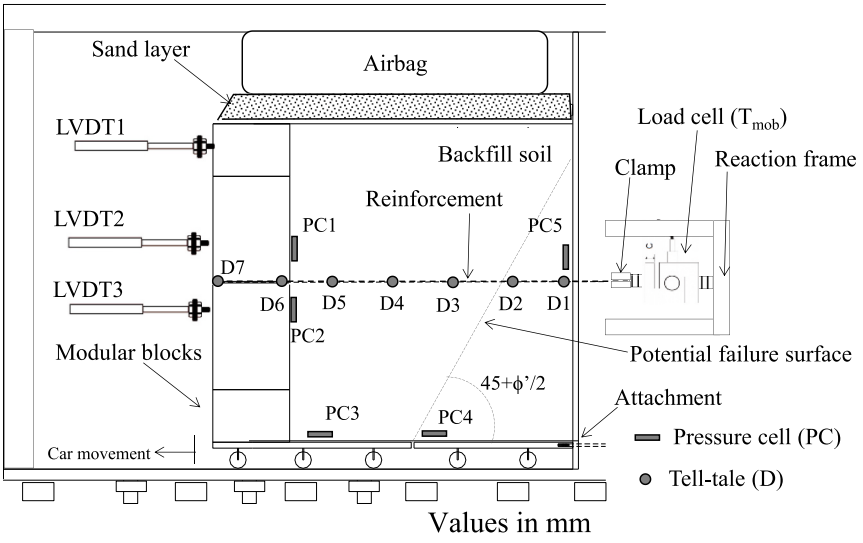

Fig. 2. Testing setup and instrumentation.

simulate a perfectly bonded anchoring length. A load cell captures the tensile load at the geosynthetic end anchored in soil, which is assumed as the load developed primarily due to the earth pressures acting at the reinforced layers excluding the down-drag effect or any other caused by reinforcement distortion at the soil-geogrid-block interface. This load source, referred to herein as T_{mob}, will be compared to the loads developed at the connection (T_o) along the reinforcement length embedded between modular concrete blocks. Earth Pressure Cells (PC) monitor the development of lateral earth pressures behind the modular blocks (PC1 and PC2). Another PC monitors the back of the reinforced soil mass, which is assumed as the lateral earth pressure acting specifically at the soil anchored length (PC5). If a potential failure surface of Rankine's theory is assumed, the failure surface location in Fig. 2 is near the load measuring point, indicating that T_{mob} may be considered as the maximum tensile load mobilized along the reinforced unit cell. Instrumentation results discussed later will prove this hypothesis.

Additional PC monitor vertical earth pressures at the base of the reinforced soil mass (PC3 and PC4). Pressure cells were calibrated inside the test box, into which the unreinforced fill material adopted in this investigation was placed in contact with the rigid bottom. The instrumentation also includes potentiometer-type 'tell tales' (Portelinha and Zornberg, 2017) for measurement of geosynthetic internal displacements. Three linear displacement transducers located outside the box were used to measure the displacement of the modular block facings. The system in its entirety and instrumentation program are detailed in Fig. 2. The image in Fig. 3 also shows the test apparatus.

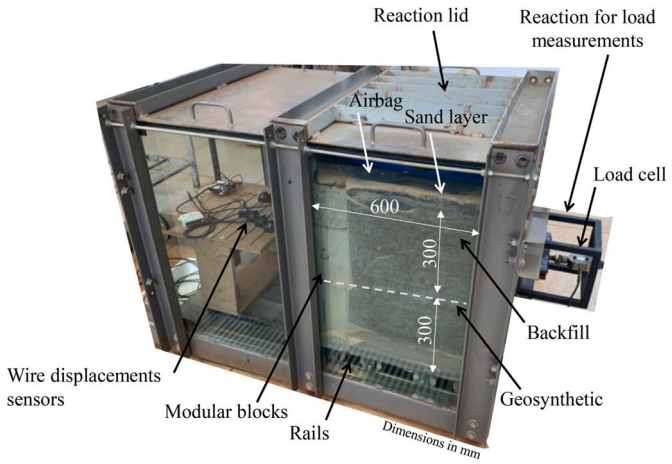

Fig. 3. Image of equipment.

2.2. Materials

In this study, a medium to coarse clean sand was used to construct the reinforced soil model. The sand is classified as poorly graded sand (SP) according to the Unified Soil Classification System (USCS). For this soil, a specific gravity of 2.67 was determined, as well as dry unit weight values of 17.6 kN/m^3 (maximum) and 15.7 kN/m^3 (minimum) corresponding to minimum and maximum void ratios of 0.52 and 0.7, respectively. A dry sieve analysis was conducted according to ASTM D6913M-17 and the resultant soil grain size distribution is shown in Fig. 4. Direct shear tests were performed at a relative density of 85% using a displacement rate of 1.25 mm/min and normal stresses of 50, 100, 150 and 200 kPa. Based on the results obtained from these direct shear tests, an internal friction angle of 30°, forcing origin to zero, was defined for the sandy soil. Direct shear test results are presented in Fig. 5. The shear strength behavior observed is typical of compacted sand.

A uniform gravel with an average grain size of 10 mm was used as fill material for the modular block facing wall. Direct shear tests of this material indicated a friction angle of 48°. A back facing gravel drain was not adopted in testing to better isolate and capture the down-drag deformation using a digital image correlation technique. Using gravel behind the blocks would not only affect the images but would also add complexity to the data interpretation. However, because most modular blocks are built with a face drain, this testing model represents a worst-case down-drag scenario. Fig. 6 shows dimensions of the facing block used and a frontal view of the facing wall.

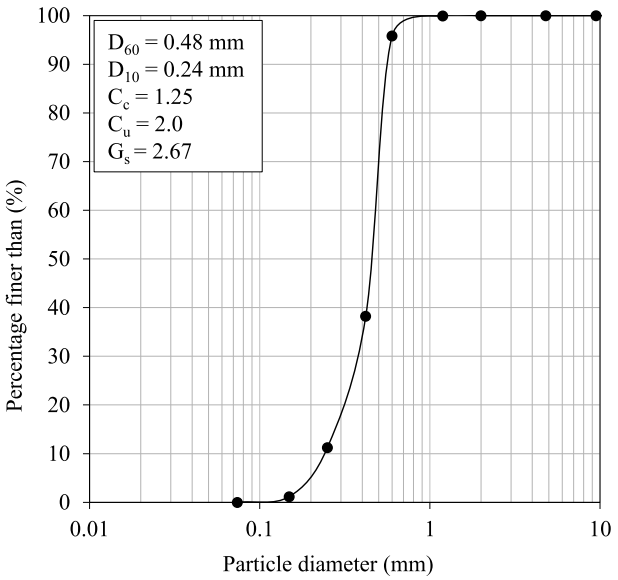

Fig. 4. Grain size distribution of sand used in tests.

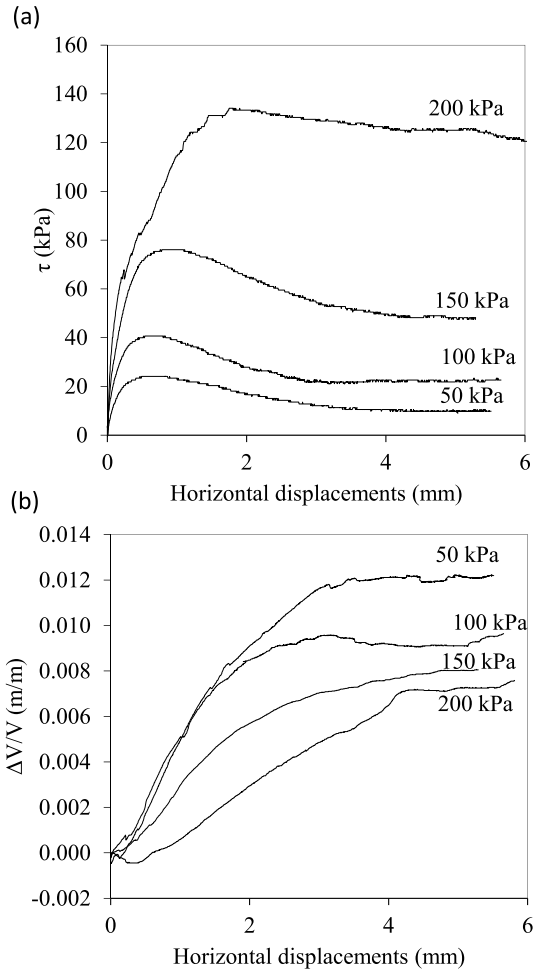

Fig. 5. Results of direct shear tests of infill sand: (a) shear stress *versus* horizontal displacements; and (b) volumetric change *versus* horizontal displacements.

The geosynthetic reinforcement used in the test involved a Polyvinyl Alcohol (PVA) woven geogrid, which was selected based on the maximum lateral pressure to be mobilized by the reinforcement in the test and the expected deformation level. The larger the relative deformation among the materials used in the model, the more difficult the DIC analysis. While polyester and uniaxial HDPE geogrids have been used more often in segmental GMSE walls, PVA geogrids have been applied in specific situations such as in very tall or load carrying structures. Table 1 summarizes the physical and mechanical properties of the geosynthetic used herein. The test specimens were 600 mm long and 700 mm wide.

2.3. Quantification of soil mass displacements

A transparent lateral wall was used to facilitate monitoring the path of soil particles during testing. This transparent wall enables the visualization of particle movements in general as well as those adjacent to the geosynthetic reinforcement layers.

Processing of images collected during testing allowed for determination of the displacement field within the soil mass at different times during testing. In addition, visualization of the differential settlement between facing and fill, as well as the associated down-drag deformation

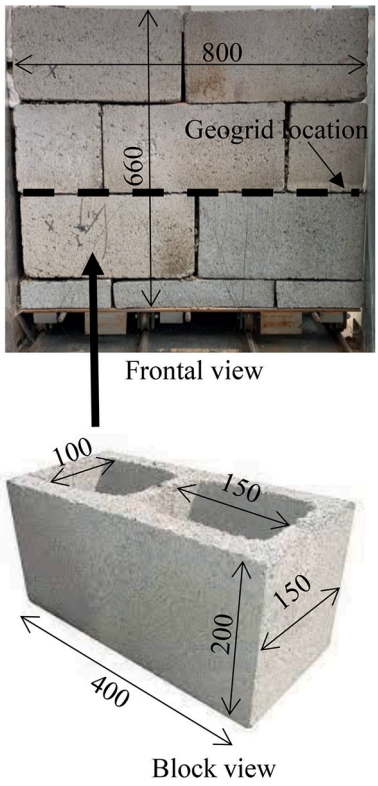

Fig. 6. Images of block facing wall (values in mm).

Table 1
Physical and mechanical properties of geosynthetics used in tests.

Properties	Standard specification	WGG
Polymer	–	PVA
Thickness (mm)	ASTM D5199	2.2
Ultimate tensile strength (kN/m)	ASTM D4595/D6637	36.4
Elongation at failure (%)	ASTM D4595/D6637	5.8
Tensile strength at 2% strain (kN/m)	ASTM D4595/D6637	11.6
MD longitudinal member width (mm)	–	3.1
CMD transverse member width (mm)	–	2.1
MD aperture size (mm)	–	11.5
CMD aperture size (mm)	–	10.3

[a] MD – Machine Direction; CMD - Cross-Machine Direction; PVA – Polyvinyl Alcohol.

of the geosynthetic at the block-reinforcement connection, provided valuable insight into the development of connection loads. A camera connected to an image tethering software program captured the transparent side of the box (Fig. 7). Tests were conducted in a dark room to reduce reflections on the window. Lighting equipment placed at the sides of the window enhanced the light intensity and uniformity. Digital Image Correlation (DIC) techniques, used to analyze the digital images obtained during testing, involve cross-correlation between successive images in an image stack. Cross-correlation identifies the best match amongst targets (sub-image or group of pixels) in consecutive images by comparing each image to the preceding one. Matching enables motion detection (movement, deformation, velocity and acceleration profiles). Details on this technique are found in Morsy et al. (2019) and Ezzein and Bathurst (2014). Black seeding particles were added to the soil to provide additional color contrast to the sand and thus improve images for DIC analysis at the interface with the transparent wall. Fig. 7a shows a lateral wall image during testing, while Fig. 7b illustrates displacement contours following DIC analysis using the software GOM correlate Pro®.

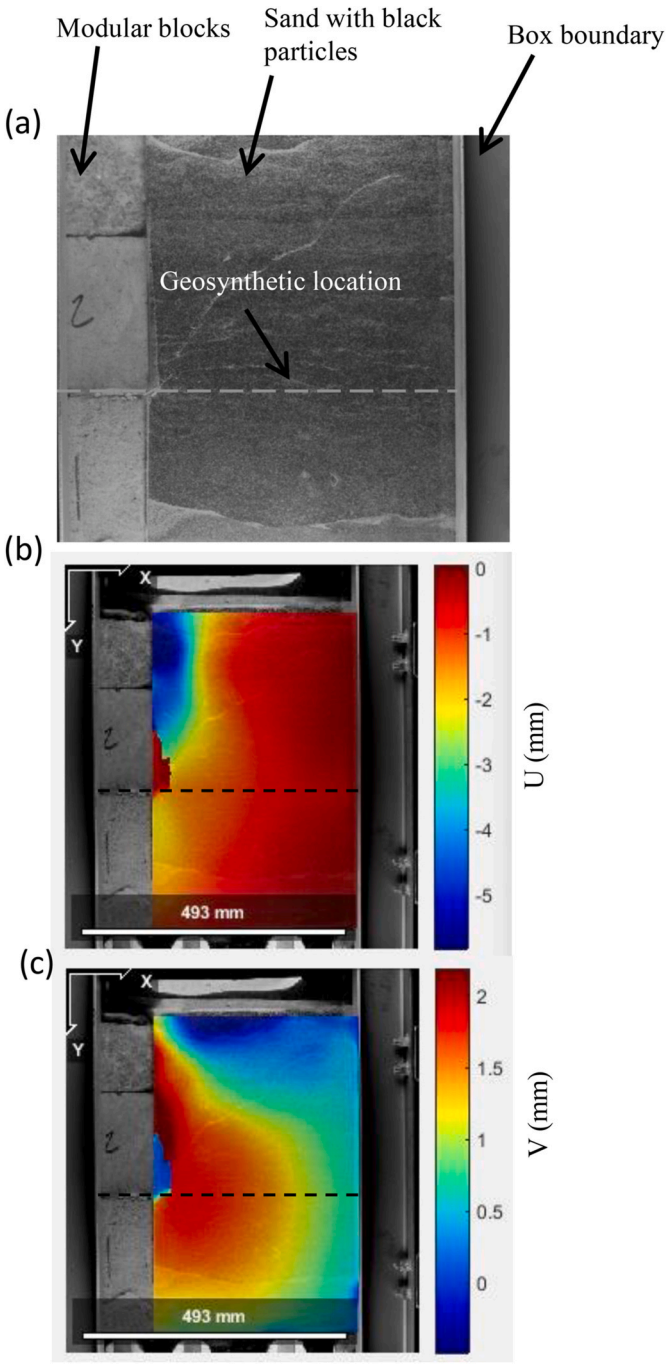

Fig. 7. Image analysis: (a) lateral transparent wall of test box with fill soil mixed with black seeding particles for DIC analysis; (b) contours of horizontal displacements; and(c) vertical displacements obtained through DIC analysis.

2.4. Construction of the model

Preparation of a soil-reinforcement layer in the test box involved initial construction of the lower sandy soil layer by pluviating the fill particles through a stack of sieves to achieve a target unit weight of 16 kN/m^3. Before depositing the soil, a thin plastic sheet was placed to minimize friction between the soil and cart surfaces. The pluviation apparatus consisted of a sand hopper with a perforated base mounted on a 1.4-m-high funnel containing the sieves. The geosynthetic specimen was embedded between upper and lower 150-mm-thick soil layers. To facilitate plane strain test conditions, adhesion between the box sidewalls and soil was minimized by using a double layer of a transparent

latex sheet and thin layer of silicon grease to create a lubrication layer at the interface. Surcharges were applied in increments of 20 kPa for 5-min periods until a final value of 180 kPa was reached. The internal and front wall displacements, lateral soil pressures and reinforcement tensile loads were recorded during each surcharge stage.

3. Results

3.1. Evaluation of displacements at the geogrid-block connection

In this study, the displacements of the modular concrete facing and along the geogrid reinforcement were monitored and evaluated. Displacements were externally monitored at three elevations along the facing, as illustrated in Fig. 2 (LVDT1, LVDT2 and LVDT3). One Linear Variable Differential Transformer (LVDT), LVDT3, was positioned 150 mm from the base of the reinforced layer system (below the geogrid layer) and two additional LVDT were positioned at distances of 350 mm (LVDT2) and 550 mm (LVDT1) from the base (above the geogrid layer). The objective of this layout was to capture the relative displacements between concrete blocks (both below and above the geogrid layer) or outward movements of the facing wall. Load-displacement results during testing are presented in Fig. 8. Specifically, the load results shown in Fig. 8a correspond to the reinforcement loads measured using the load cell at the back of the reinforced system (mobilized load T_{mob}), which primarily results from lateral earth pressures developed from the surcharge pressure at the corresponding layer. The T_{mob} values mobilized during the test are plotted against the facing displacements monitored by the external LVDT. Typical load-displacement curves can be seen in the figure, with a peak load of 5 kN/m at the back of the reinforced system and lateral displacements on the order of 10–15 mm for blocks located above the reinforcement layer (LVDT1 and LVDT2 of Fig. 2), and a reduced value of 3 mm for the blocks below (LVDT3), indicating the bending of the facing wall.

Fig. 8b shows the displacement profiles at each surcharge stage during testing. In general, the facing blocks moved outward, with greater movement observed in the layer above the geogrid. This pattern of facing deformation is consistent with the expected stress distribution, where lateral stresses are typically higher closer to the surcharge application. Furthermore, the contribution of the geogrid in mobilizing stresses may also affect block displacements below the geogrid layer. Fig. 9 shows pictures of the system taken from the lateral transparent wall before (Fig. 9a) and after (Fig. 9b) applying a surcharge of 180 kPa. Although the load-displacement curve indicates a peak (Fig. 9a), connection failure is not evident in the figure. Images corroborate the bending behavior captured by the LVDT, showing no significant relative displacements between blocks. A similar displacement distribution pattern was reported by Gebremariam et al. (2020) for a GRS-Integrated Bridge System (GRS-IBS) after the placement of a slab load. Additionally, while the facing continuously displaced outward, the T_{mob} showed a decreasing trend with an increase in displacement, which may indicate proximity to a block-geogrid connection failure.

Fig. 10a depicts the displacements measured along the length of the geogrid using tell-tales. The strain distribution along the reinforcement can be determined using internal displacement measurements, which can in turn be used for a load distribution assessment. In this study, displacements were measured both at points where the geogrid was embedded in the soil and at points where the geogrid was placed between concrete blocks. The telltales D6 and D7, indicated in Fig. 2, correspond to those inserted at the interface between blocks: D7 is located at the front of the block facing while D6 is within the interface

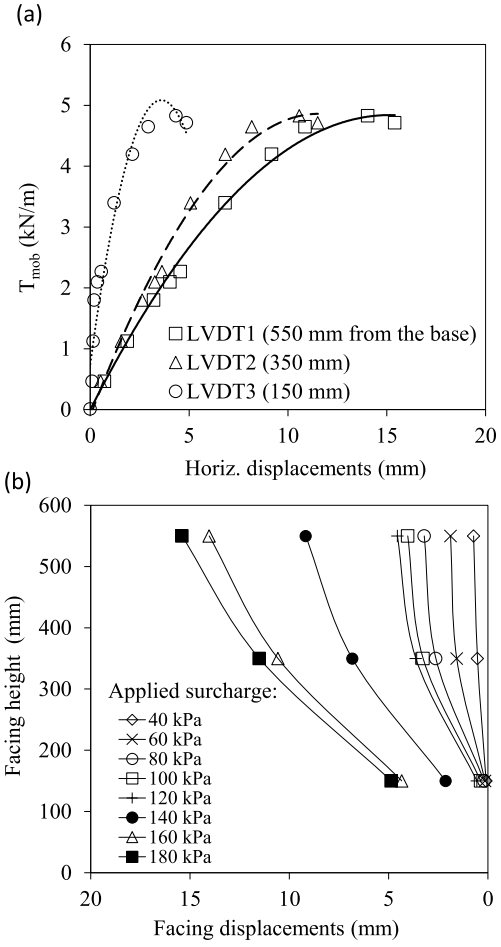

Fig. 8. Mobilization of facing lateral displacements: (a) mobilized load (T_1) versus facing displacement at different elevations; and (b) displacement profiles along the facing height at different surcharge stages.

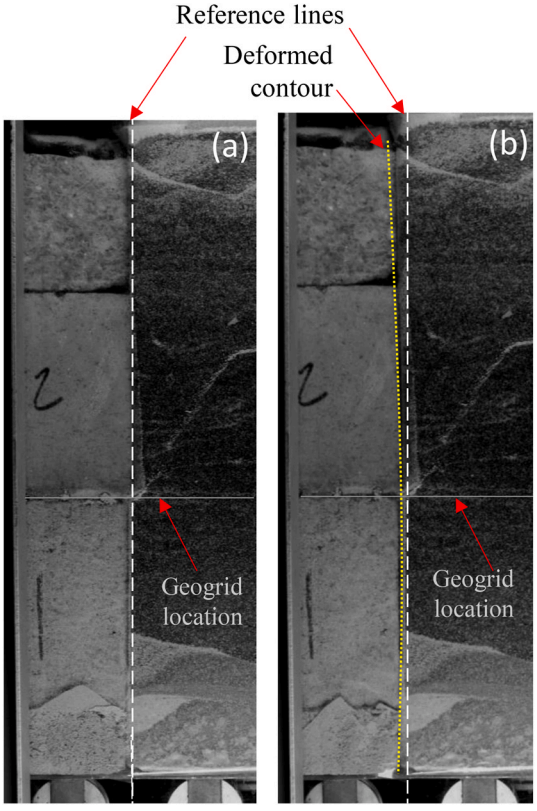

Fig. 9. Images of facing taken from transparent lateral wall: (a) at first surcharge stage; and (b) after 180 kPa of surcharge.

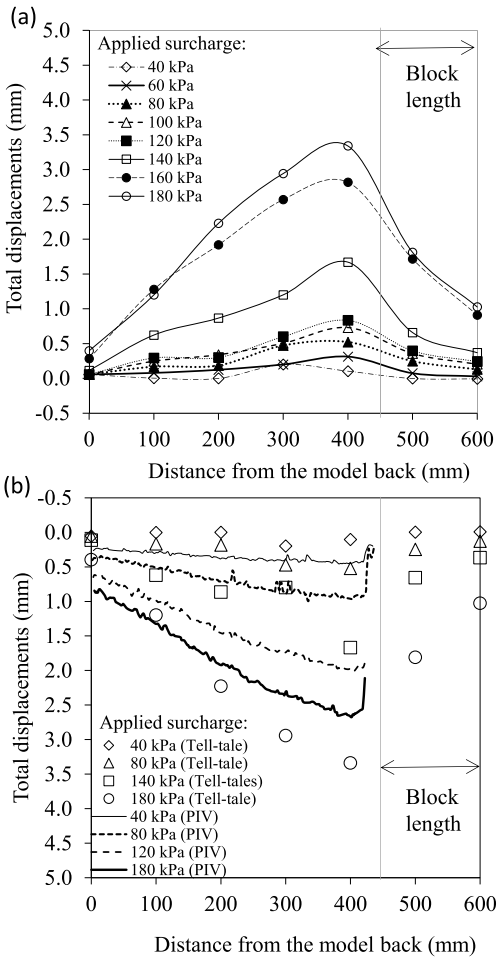

Fig. 10. Displacement distributions along geogrid length: (a) measured by tell-tales; and (b) measured using DIC and comparison to tell-tales.

between blocks at the back. The tell-tales attached along the geogrid capture total displacements, including horizontal displacements generated by lateral stresses and vertical displacements due to relative settlement between the soil and block facing. The total displacements captured within the blocks were primarily horizontal as vertical displacements were negligible. The data in Fig. 10a show increased displacements toward the face but significant decreases at points within the concrete block interface. The displacements measured in the reinforced backfill soil include both vertical and horizontal components because the soil is the only part of the system that can deform in response to the surcharge stress imposed, resulting in significantly higher values. Displacements typically increased with surcharge increments, with higher rates observed within the backfill soil. Internal displacements within the blocks (at D6 and D7) remained similar at lower surcharge levels, indicating mobilization of the anchorage layer between blocks. However, at higher surcharge levels, displacements inside the blocks decreased toward the front, suggesting relative horizontal displacement between the geogrid and blocks. The notably greater displacements recorded near the back can be attributed to the differential settlement in this region. When a differential settlement occurs due to the differing rigidity of the facing and backfill soil, geogrid dragging is expected to occur if adequately anchored between blocks. In the literature, this phenomenon has been documented to produce down-drag forces (Soong and Koerner, 1997; Morsy, 2021). Significant differential settlements are typically observed only at vertical pressures exceeding 100 kPa.

Fig. 10b compares the total displacements captured via tell-tales with those obtained from image analysis. This comparison indicates good agreement between both measurement systems, although the tell-tale measurements were slightly higher than those obtained via the DIC approach. It is possible the displacement levels were slightly different because the images for displacement analysis were captured at the lateral wall, while the tell-tale measurements were obtained from the center plane of the reinforced soil mass. However, as both measurement approaches resulted in similar trends, image analysis proved valuable for this investigation. Additionally, as more complete displacement fields were obtained, the use of digital image analysis became advantageous to quantify the differential settlements in the back of the block facing.

3.2. Evaluation of displacements collected through visualization

Digital image analysis was employed to analyze vertical and horizontal displacement measurements collected through images captured at each loading stage near the geogrid-facing block connection.

Fig. 11 presents the distribution of horizontal, vertical and total displacements along the length of the geogrid obtained through digital image analysis. These data facilitate the quantification of down-drag deformation along the length of the reinforcement as well as the interpretation of loads mobilized along the geosynthetic. Fig. 11a depicts horizontal displacements increasing toward the face. Additionally, uniform increases in vertical displacements can be observed in the initial surcharge stages (20 kPa and 40 kPa), as illustrated by the results presented in Fig. 9b. As vertical stress increased with subsequent surcharge stages, vertical displacements also increased, with more pronounced changes occurring at the back of the facing blocks, capturing the relative vertical settlement, which induced geogrid down-drag in this section of the wall. Greater differential settlements across the reinforced system were observed at higher applied surcharge levels, caused by localized asymmetric soil deformation. According to Soong and Koerner (1997), out-of-plane stresses in the reinforcement can be induced by post-construction settlement of the backfill relative to a stationary facing system. In practical applications, out-of-plane stresses may arise due to soil loss, foundation settlement, inadequate compaction near the facing or poor backfill compaction. Outward rotation to achieve active stress conditions and hydro compaction, where water infiltration causes soil consolidation, are also potential causes of out-of-plane stresses and subsequent down-drag deformation of the reinforcement. In this investigation, out-of-plane stresses were intentionally induced by restricting settlement of the block facing wall and allowing the backfill soil to deform in response to the imposed surcharge stress. Foundation settlements were not assumed in testing. The down-drag effect could be observed even under controlled soil compaction.

The quantification of horizontal and vertical displacements along the length of the geogrid also facilitates calculation of down-drag deformation across surcharge stages. The angle of the reinforcement at the facing (ξ) was utilized by Morsy (2021) to quantify the down-drag deformation. Fig. 12 illustrates changes in the down-drag angle along the geogrid at the end of each surcharge stage. The down-drag angle ranged from 10 to 25° at 20 kPa and 40 kPa of surcharge, respectively, and increased from 28 to 42° after the application of 160 kPa of surcharge. The difference in down-drag angles observed from the back toward the facing were significantly greater at 180 kPa of surcharge due to the high surcharge stress level, which led to large backfill soil deformation and resulted in significant relative movement between the block wall and backfill soil. In this scenario, the down-drag deformation was substantial and led to an increase in the down-drag angle.

3.3. Analysis of the connection loads developed at the geogrid-block interface

Two distinct approaches were employed herein to determine the connection loads. Pressure cells positioned above and below the reinforcement layer (PC1 and PC2 in Fig. 2) measured the lateral earth pressure at the back of the blocks, which was subsequently utilized to

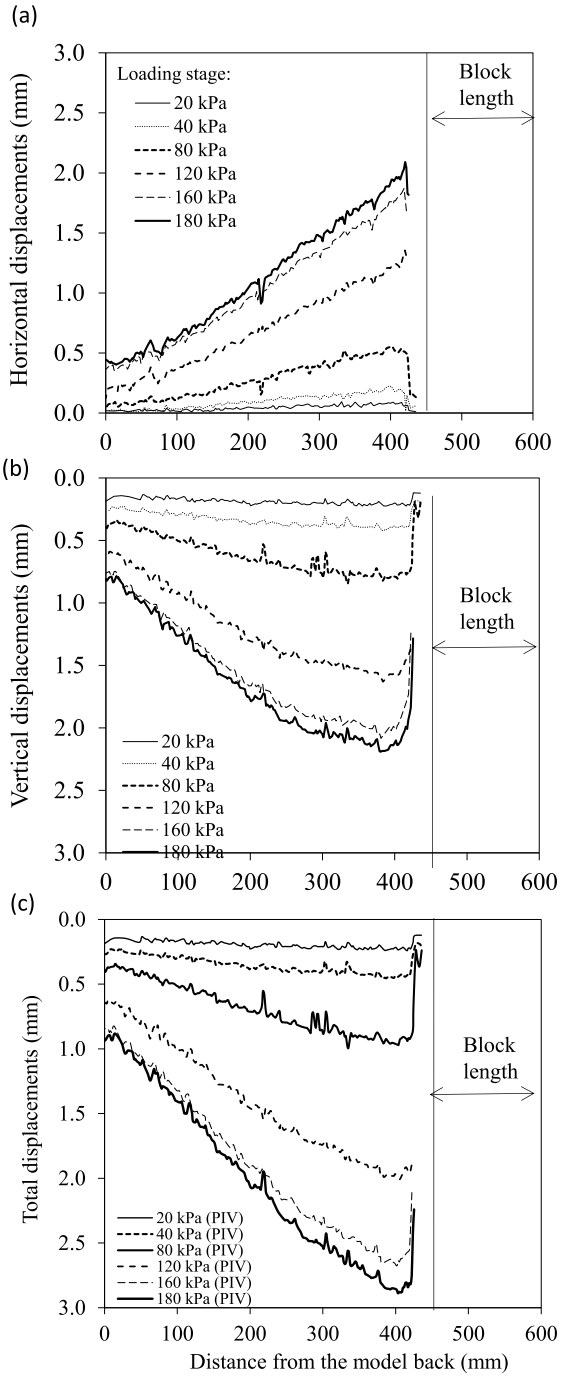

Fig. 11. Displacement field captured by digital image analysis: (a) horizontal displacements along geogrid length; (b) vertical displacements; and (c) total displacements.

compute the horizontal load by dividing it by the tributary area (vertical spacing). With this method, the connection load derived specifically from lateral earth pressures exerted behind the wall facing was calculated. Down-drag loads are neglected in this method. Likewise, the strain calculated from the horizontal displacements measured at the connection, from the geogrid length embedded between blocks in particular, was also utilized to calculate the mobilized tensile load based on the secant stiffness obtained from constant-rate load-elongation tests. Since

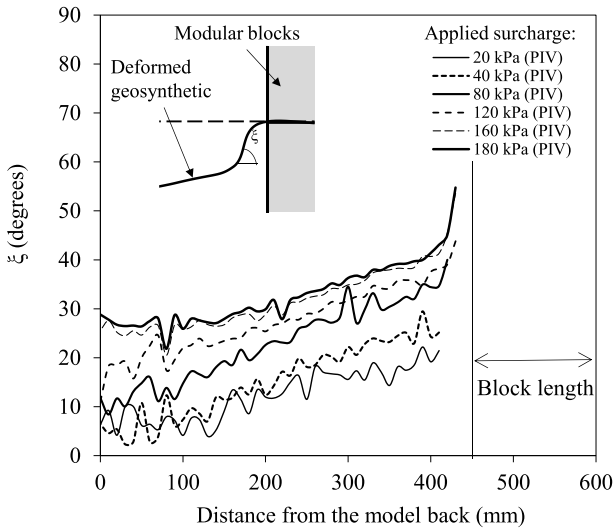

Fig. 12. Effect distribution of down-drag angle along geogrid length.

the test is conducted over a relatively short duration (surcharge stages lasting less than 1 h), utilizing constant-rate tests would slightly underestimate loads compared to rate-dependent tests due to the reduced time-dependent strain behavior of PVA yarns (Kongkitkul et al., 2007). However, the differences are deemed negligible for the purposes of this study.

Using the secant stiffness of the geogrid to determine mobilized loads allows for the consideration of contributions from two sources: lateral earth pressure and down-drag effects. However, the maximum connection load calculated using geogrid strain was observed to be located at the first measurement point outside at the back of block facing interfaces. Therefore, the distribution of reinforcement loads along the length of the geosynthetic was also calculated using the total strains obtained through tell-tales and DIC. Load distributions obtained from tell-tales along the geogrid length are displayed in Fig. 13a, while Fig. 13b depicts load distributions from DIC analysis. Strains within the block interface could not be obtained via image gathering. Based on the location of the potential failure surface imposed by the equipment, as indicated in Fig. 2, the mobilization of maximum tensile loads potentially occurred approximately 150 mm from the back wall. Although the load calculation methods demonstrated different behaviors, both exhibited similar levels of mobilized loads and consistent peak locations. Peak loads developed approximately 300 mm from the back of the facing block (150 mm from the model back) in most surcharge stages, indicating the location of a potential failure surface. However, a secondary load concentration was also observed internally at the block-to-block interface. A maximum reinforcement load between 100 mm and 250 mm from the model back was observed for the first surcharge stages (up to 120 kPa). At 40 kPa of surcharge, the connection load was close to zero. When the surcharge increased to 80 kPa, the connection load was observed to reach 80% of the maximum load measured within the backfill soil, which increased to approximately 100% as 120 kPa was applied. For higher surcharges, the connection load exceeded the maximum load mobilized by geosynthetic by approximately 1.5 times. These results indicate that if the connection loads were primarily developed by earth pressures, they could, at most, equal the maximum mobilized load at the potential failure surface. These findings agree with current standard practices (AASHTO, 2020; Berg et al., 2009). However, because this behavior is observed under lower applied surcharges, the sudden peak loads observed within the block interface indicate the development of down-drag forces under elevated surcharge pressures. The loads measured via load cells attached to the back of the unit cell were similar to the values measured internally using tell-tales, thus validating the assumption that T_{mob} can be considered as (or close to)

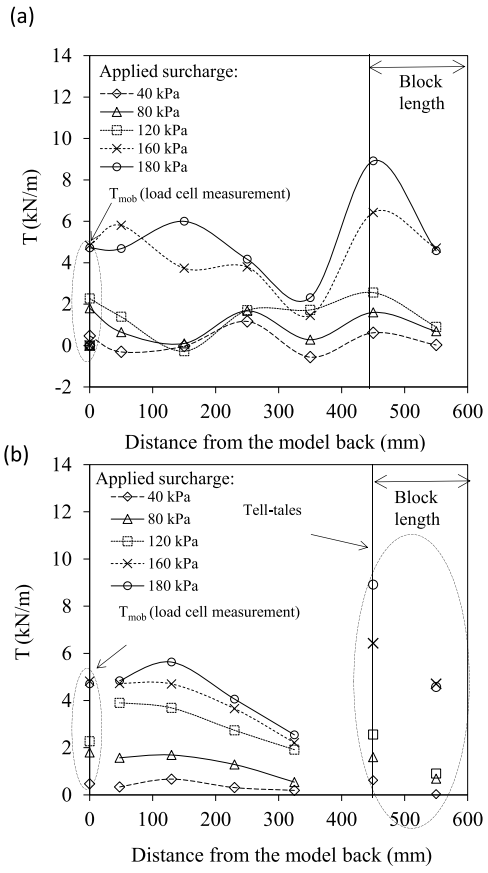

Fig. 13. Distribution loads mobilized along geosynthetic reinforcement.

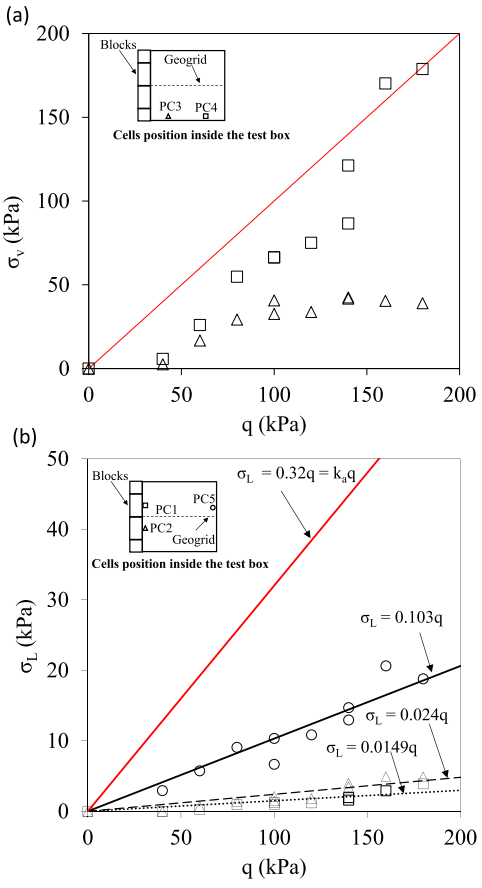

Fig. 14. Stresses measured by pressure cells during testing: (a) vertical stresses at base; and (b) horizontal stresses at facing and back wall versus applied vertical stress.

T_{max} developed along the potential failure surface, as indicated in Fig. 2.

Pressure cells were also installed to obtain vertical earth pressures (PC3 and PC4 in Fig. 2). The actual earth pressures measured during testing are evaluated in Fig. 14. Fig. 14a compares the applied surcharge to the vertical earth pressures measured via PC. PC3 is located at the base, near the back of the block facing, while PC4 is 200 mm from the back wall of the test box. The measured vertical earth pressures were generally lower than the applied pressure, and the values measured by PC4 were greater than those measured by PC3 (near the face). Under the surcharge, the geogrid experienced greater tension due to the localized down-drag effect near the face. A tensioned geogrid in this area, caused by down-drag deformation, may absorb a portion of the applied vertical pressure. However, the bulk of this behavior can be attributed to the friction between the soil and blocks, resulting in lower vertical stresses near the back-facing wall. Beyond the length of the reinforcement affected by down-drag deformation, the vertical earth pressure values were similar to the applied pressures, as indicated by PC4.

Lateral earth pressures measured at the back of the facing blocks are depicted in Fig. 14b. The measured lateral earth pressures (σ_L) are plotted against the applied surcharge (q). The slope of the curves can be interpreted as the earth pressure coefficient (K) acting on the reinforced unit cell. Pressure cells PC1 and PC2 are located at the back of the blocks that interface with the geogrid. PC1 is positioned at the block above the reinforcement layer while PC2 is located on the back of the block below the reinforcement layer. PC5 is located at the back wall of the test box, near the point where the maximum tensile load was measured via load cell. Lateral earth pressures measured by PC5 can be understood as those developed along the potential failure surface. As expected, both PC1 and PC2 recorded similar lateral earth pressure values during testing. A comparison of the active earth pressure defined by Rankine (red line), in which $K_a = \tan^2(45\text{-}\varphi/2)$, with the values measured by PC5 highlights the conservatism of Rankine, as reported by many authors in the literature (Portelinha et al., 2014; Bathurst et al., 2008a). This is expected as Rankine's lateral earth pressures assume the soil is yielding, while the soil is under working stress conditions in the test. Comparatively, lateral earth pressures measured at the face by PC1 and PC2 were significantly lower than those measured by PC5, indicating that lateral stresses at the connection were five to 10 times lower than those mobilized by reinforcements along the potential failure surface. Among the sources contributing to the development of connection loads, the results indicate that lateral earth pressures at the face contributed only 20% to the total for the facing conditions imposed in the test. The remaining 80% can potentially be attributed to down-drag deformation, which is not captured by the earth PC. To provide a better understanding, Fig. 15 compares the connection loads (T_o) calculated using the lateral earth pressures measured by PC1 and PC2 with those obtained from tell-tales. In this figure, the different determinations of T_o are plotted against the T_{mob} to quantify the required loads at reinforcement connections to the wall face relative to the maximum mobilized load. The data demonstrate that the use of lateral earth pressures to calculate connection loads underestimates the conditions, which involve relative settlements between the backfill soil and facing. The results from PC approximate the connection loads (T_o) calculated using tell-tales only at lower values of T_{mob} (up to 2 kN/m), which were captured at lower surcharge levels and, consequently, lower or zero relative displacement between soil and block wall. At T_{mob} values greater than 2 kN/m, T_o values calculated using PC were significantly lower than those measured by tell-tales. Moreover, the connection loads obtained from PC accounted for only 53% of the mobilized tensile load (T_{mob}). This discrepancy emphasizes

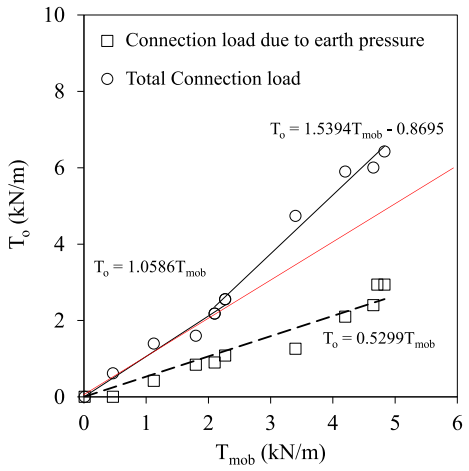

Fig. 15. Connection loads (T_o) from different sources *versus* mobilized loads (T_{mob}).

that earth PC do not capture down-drag forces, which leads to an underestimation of the connection loads at the face. Conversely, the connection loads calculated using the reinforcement strains at the connection revealed that the connection load between the geogrid and modular blocks was equal to T_{mob}, as is often assumed in design analysis (Elias et al., 2001), at lower surcharge levels. However, the data from this investigation indicate that the connection load can be 1.5 times greater than T_{mob} for higher vertical pressure levels, conditions in which down-drag deformation is intensified (Fig. 12).

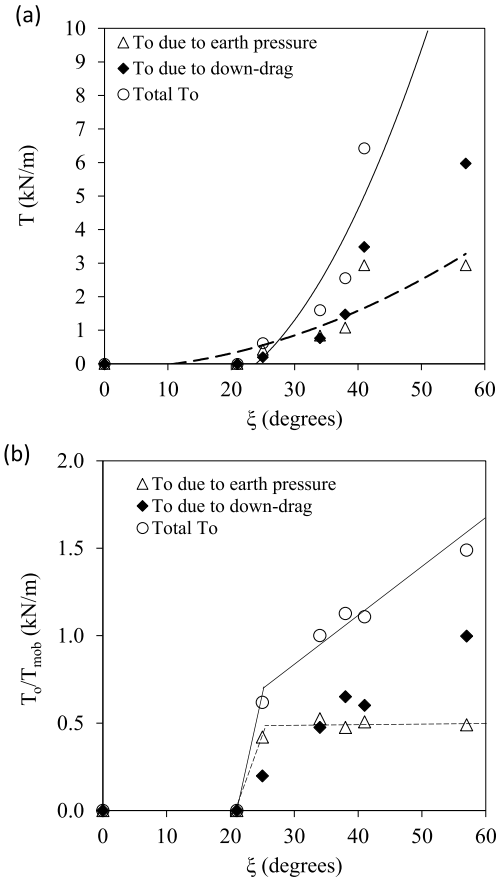

Fig. 16. Effect of down-drag angle on connection load at facing: (a) connection loads calculated using pressure cells and tell-tales versus down-drag angles; and (b) T_o/T_{mob} versus down-drag angles.

To better illustrate the relationship between connection loads and down-drag deformation, Fig. 16a plots the down-drag angle against the connection loads developed during testing to compare the different sources of connection loads. Similarly, Fig. 16b depicts the ratio of T_o (connection load) to T_{mob} (load mobilized at the potential failure surface) to calculate the percentage of loads carried at the connection relative to the load mobilized at the potential failure surface. The results from Fig. 16a show a significant increase in the total connection load, incorporating both down-drag and earth pressure influences, with the down-drag angle. The down-drag angle can be observed to have moderately influenced the connection load due to earth pressure, which reveals that most of the total connection load resulted from down-drag deformation. However, lateral earth pressure has an influence on connection loads similar to down-drag deformation, particularly for down-drag angles less than 30°. The findings in Fig. 16b indicate that connection loads should be assumed as equal to T_{mob} when the down-drag angle is less than 40°, corresponding to the 80 kPa applied surcharge, and can exceed T_{mob} at greater angles. Using measured lateral earth pressures to calculate T_o indicates that it is 50% of T_{mob}. The observations derived from Fig. 16b partly support the current standard practices. The results suggest that adopting 50% of the maximum tensile load for lower surcharges and 100% for higher levels of vertical surcharges is reasonable and also consistent with actual instrumented full-scale wall (SR-18 walls) responses reported by Yu et al. (2016). However, the standard practices do not address that, for high levels of surcharge, the connection load can surpass the maximum tensile load in the backfill due to the development of out-of-plane stresses. In this investigation, connection loads increased by 50% relative to the maximum tensile load with an increase in the down-drag angle. The analysis conducted in this subsection indicates that relative settlements can be critical to the facing stability of GRS walls. Therefore, analytical frameworks to predict down-drag forces developed at facing connections are recommended to advance design analysis.

4. Concluding Remarks

In this study, loads developed at the connection between a geogrid and modular block facing were evaluated using a laboratory testing device created to properly simulate the mechanisms involved at the facing of a GMSE wall. The test apparatus consists of a reinforced unit cell that facilitates the simulation and monitoring of stress transference at the face and allows for the quantification of the required connection loads in GMSE walls. The testing program involved a geogrid reinforcing a clean sand backfill, which was connected frictionally to a modular concrete block facing. An extensive instrumentation program was used to capture vertical and lateral earth pressures, internal and external displacements, geogrid strains and loads mobilized at the facing of a geosynthetic-reinforced unit cell when subjected to different surcharge levels. The testing mechanism adopted in this experimental program consistently simulated the mechanisms involved in a facing-geogrid-soil interface in terms of stress-strain responses and transference of stresses. In addition, image gathering and digital image correlation proved to be valuable tools to fully evaluate the displacement distribution and capture down-drag deformations.

The results of this investigation demonstrate that facing connection loads should not be understood as resulting only from earth pressures, but also due to additional tensioning caused by the relative displacements between the backfill material and facing wall that led to down-drag deformation. Calculations based on earth pressures were observed to underestimate connection loads for the modular blocks adopted when differential settlements developed. Consequently, approaches based on earth pressure theories should not be the sole source of load in situations where out-of-plane stresses are induced in the reinforcement due to post-construction settlement of the backfill relative to the stationary facing.

The down-drag deformation of the reinforcement induced significant

facing connection loads, the magnitude of which is dependent on the magnitude of down-drag deformation. Connection loads were observed to vary from 50% to 100% of the maximum load mobilized along the reinforcement length anchored in soil, depending on the level of applied surcharge, as is often assumed in design analysis. This assumption was found to be realistic primarily when the down-drag angle was less than 40°. Under surcharges that led to down-drag angles over 40°, connection loads were found to significantly increase with the down-drag angles, reaching values 1.5 times greater than the maximum reinforcement load.

This study investigated the mechanisms and contributing factors in the evolution of connection loads, with a specific focus on understanding the effect of relative settlement between the backfill and block facing wall. The data should not be immediately applied to the practice of segmental GMSE walls as more rigorous testing to replicate the real-world conditions of segmental GMSE practice must be performed. Nonetheless, these results contribute relevant details to many cases involving facing connection stability failure. However, further research is recommended to identify and quantify the contribution of the many variables and mechanisms involved in development of connection loads, including block configuration, infill material for the block and behind the block, and the soil behind the gravel face drain. Other important variables to be investigated are also related to the development of down-drag forces such as the type of compaction, hydro consolidation of the backfill soil and type of reinforcement.

CRediT authorship contribution statement

F.H.M. Portelinha: Writing – review & editing, Writing – original draft, Supervision, Resources, Project administration, Methodology, Funding acquisition, Formal analysis, Data curation, Conceptualization. **P.V.C. Figueiredo:** Visualization, Validation, Methodology, Investigation. **J.G. Zornberg:** Writing – original draft, Methodology, Conceptualization.

Data availability

Data will be made available on request.

Acknowledgements

The authors thank to the Higher Education Personnel Improvement Coordination - Brazil (CAPES) - Finance Code 001, for post-doctoral scholarships to the first author, which allow the development of this research. Special thanks to the Laboratory of Geotechnics and Geosynthetics of the Federal University of Sao Carlos (UFSCar), Brazil, for the facilities.

References

AASHTO, 2020. AASHTO LRFD Bridge Design Specifications, ninth ed. Association of State Highway and Transportation Officials, Washington, D.C.

Adams, M., Nicks, J., 2018. Design and Construction Guidelines for Geosynthetic Reinforced Soil Abutments and Integrated Bridge Systems, vol. 228.

Allen, T.M., Bathurst, R.J., 2014a. Design and performance of 6.3-m-high block-faced geogrid wall designed using K-stiffness method. J. Geotech. Geoenviron. Eng., 04013016 https://doi.org/10.1061/(ASCE)GT.1943-5606.0001013.

Allen, T.M., Bathurst, R.J., 2014b. Performance of an 11 m high block-faced geogrid wall designed using the K-stiffness method. Can. Geotech. J. 51 (1), 16–29. https://doi.org/10.1139/cgj-2013-0261.

Bathurst, R.J., 2005. NCMA Segmental RetainingWall Seismic Design Procedure: Supplement to Design Manual for Segmental Retaining Walls, first ed. National Concrete Masonry Association, Herndon, VA, USA, p. 187pp. Third Print.

Bathurst, R.J., Huang, B., 2010. A geosynthetic modular block connection creep test apparatus, methodology, and interpretation. Geotech. Test J. 33 https://doi.org/10.1520/GTJ102491.

Bathurst, R.J., Simac, M.R., 1993. In: Cheng, S.C.J. (Ed.), Laboratory Testing of Modular Unit-Geogrid Facing Connections. STP 1190 Geosynthetic Soil Reinforcement Testing Procedures. American Society for Testing and Materials (Special Technical Publication), pp. 32–48, 1993.

Bathurst, R.J., Simac, M.R., Berg, R.R., 1993. Review of NCMA segmental retaining wall design manual for geosynthetic reinforced structures. Transport. Res. Rec. 1414, 16–25.

Bathurst, R.J., Vlachopoulos, N., Walters, D.L., Burgess, P.G., Allen, T.M., 2007. Reply to the discussions on "The influence of facing rigidity on the performance of two geosynthetic reinforced soil retaining walls". Can. Geotech. J. 44 (12), 1484–1490.

Bathurst, R.J., Althoff, S., Linnenbaum, P., 2008a. Influence of test method on direct shear behavior of segmental retaining wall units. ASTM Geotechnical Testing Journal 31 (No. 2), 9.

Berg, R.R., Christopher, B.R., Samtani, N.C., 2009. Design of Mechanically Stabilized Earth Walls and Reinforced Soil Slopes – Volume I. Federak Highway Asministration (FHWA-NHI-10-24), Washington, D.C.

Collin, J.G., 1997. Design Manual for Segmental Retaining Walls, third ed. National Concrete Masonry Association, Herndon, VA.

Elias, V., Christopher, B.R., Berg, R.R., 2001. Mechanically Stabilized Earth Walls and Reinforced Soil Slopes Design and Construction Guidelines (FHWA-NHI-00-43). Federal Highway administration, Washington, D.C.

Ezzein, F.M., Bathurst, R.J., 2014. A new approach to evaluate soil-geosynthetic interaction using a novel pullout test apparatus and transparent granular soil. Geotext. Geomembranes 42, 246–255. https://doi.org/10.1016/j.geotexmem.2014.04.003.

Gebremariam, F., Tanyu, B.F., Christopher, B., Leshchinsky, D., Zornberg, J.G., Han, J., 2020. Evaluation of required connection load in GRS-IBS structures under service loads. Geosynth. Int. 27, 620–634. https://doi.org/10.1680/jgein.20.00022.

GRI, 1991. Standard Test Method for Determining the Tensile Strength of Mechanically Anchored Geosynthetics, GRI Test Method GS−8. Geosynthetic Research Institute, Philadelphia, PA.

Koerner, R.M., Koerner, G.R., 2018. An extended data base and recommendations regarding 320 failed geosynthetic reinforced mechanically stabilized earth (MSE) walls. Geotext. Geomembranes. https://doi.org/10.1016/j.geotexmem.2018.07.013.

Leshchinsky, D., Leshchinsky, O., Zelenko, B., Horne, J., 2016. Limit Equilibrium Design Framework for MSE Structures with Extensible Reinforcement (FHWA-HIF-17-004). Federal Highway Administration, Washington, D.C.

Morsy, A.M., 2021. Analytical framework for prediction of facing connection loads in reinforced soil walls considering reinforcement downdrag. Transp. Geotech. 30 https://doi.org/10.1016/j.trgeo.2021.100537.

Morsy, A.M., Zornberg, J.G., Han, J., Leshchinsky, D., 2019. A new generation of soil-geosynthetic interaction experimentation. Geotext. Geomembranes 47, 103455. https://doi.org/10.1016/j.geotexmem.2019.04.001.

Portelinha, F.H.M., Zornberg, J.G., 2017. Effect of infiltration on the performance of an unsaturated geotextile-reinforced soil wall. Geotext. Geomembranes. https://doi.org/10.1016/j.geotexmem.2017.02.002.

Portelinha, F.H., Zornberg, J.G., Pimentel, V., 2014. Field performance of retaining walls reinforced with woven and nonwoven geotextiles. Geosynth. Int. https://doi.org/10.1680/gein.14.00014.

Riccio, M., Ehrlich, M., Dias, D., 2014. Field monitoring and analyses of the response of a block-faced geogrid wall using fine-grained tropical soils. Geotext. Geomembranes 42, 127–138. https://doi.org/10.1016/j.geotexmem.2014.01.006.

Salem, M.A., Hammad, M.A., Amer, M.I., 2018. Field monitoring and numerical modeling of 4.4 m-high mechanically stabilized earth wall. Geosynth. Int. 25, 545–559. https://doi.org/10.1680/jgein.18.00027.

Simac, M.R., 1990. Connections for geogrid systems. Geotext. Geomembranes 9, 4–6. https://doi.org/10.1016/0266-1144(90)90048-H.

Simac, M.R., Bathurst, R.J., Berg, R.R., Lothspeich, S.E., 1993. National Concrete Masonry Association Segmental Retaining Wall Design Manual, first ed., p. 250 March 1993.

Soong, T.Y., Koerner, R.M., 1997. On the required connection strength of geosynthetically reinforced walls. Geotext. Geomembranes 15, 377–393. https://doi.org/10.1016/S0266-1144(97)10016-4.

Task Force 27, AASHTO-AGC-ARTBA Joint Committee, 1990. Design Guidelines for Use of Extensible Reinforcements (Geosynthetics) for Mechanically Stabilized Earth Walls in Permanent Applications. AASHTO, Whashington, D.C.

Wu, J.T.H., 2001. Revising the AASHTO guidelines for design and construction of GRS walls. Rep. No. CDOT-DTD-R-2001-16 148.

Xu, P., Hatami, K., Jiang, G., 2020. Shaking table study of the influence of facing on reinforced soil wall connection loads. Geosynth. Int. 27 (No. 4), 364–378. https://www.icevirtuallibrary.com/doi/10.1680/jgein.20.00001.

Yu, Y., Bathurst, R.J., Allen, T.M., 2016. Numerical modelling of the SR-18 geogrid reinforced modular block retaining walls. ASCE J. Geotech. Geoenvironmental Eng. 142 (5), 04016003 https://doi.org/10.1061/(ASCE)GT.1943-5606.0001438.